Materials Today Chemistry 24 (2022) 100846

Contents lists available at ScienceDirect

Materials Today Chemistry

journal homepage: www.journals.elsevier.com/materials-today-chemistry/

The covalent functionalization of few-layered MoTe2 thin films with iodonium salts

O. Guselnikova [a, ***], J.P. Fraser [b], N. Soldatova [a], E. Sviridova [a], A. Ivanov [a], R. Rodriguez [a], A.Y. Ganin [b, **], P. Postnikov [a, *]

[a] Research School of Chemistry and Applied Biomedical Sciences, Tomsk Polytechnic University, Tomsk, 634050, Russian Federation
[b] School of Chemistry, University of Glasgow, Glasgow, G12 8QQ, United Kingdom

ARTICLE INFO

Article history:
Received 5 November 2021
Received in revised form
14 January 2022
Accepted 14 February 2022
Available online xxx

Keywords:
Transition-metal dichalcogenides
2D materials
Surface chemistry
X-Ray Photoelectron Spectroscopy
Chemical Vapor Deposition
Iodonium salt

ABSTRACT

Covalent functionalization of 2D materials provides a tailored approach towards tuning of their chemical, optical, and electronic properties making the search for new ways to graft small molecules important. Herein, the reaction with (3,5-bis(trifluoromethyl)phenyl)iodonium salt is revealed as an effective strategy for functionalization of $MoTe_2$ thin films. Upon decomposition of the salt, the generated radicals graft covalently as aryl-$(CF_3)_2$ groups at the surface of both metallic (1T') and semiconducting (2H) polymorphs of $MoTe_2$. Remarkably, the reactivity of the salt is governed by the electronic structure of the given polymorph. While the functionalization of the metallic $MoTe_2$ occurs spontaneously, the semiconducting $MoTe_2$ requires activation by light. The reaction proceeds with the elimination of oxide from the original films yielding the functionalized products that remain protected in ambient conditions, presenting a viable solution to the ageing of $MoTe_2$ in air.

Once a mere academic curiosity, atomically-thin, two-dimensional (2D) transition-metal dichalcogenides (TMDCs) have become an important class of materials capable of driving transformative changes to modern electronic and photonic networks [1–3], catalytic systems [4–6], sensing and biomedical applications [7–9]. 2D materials consist mainly of surfaces that dictate their physical properties [1]. Thus, controlling the surfaces offers exciting opportunities for future developments of 2D TMDCs as even minor changes to the surface states could have a major impact over their electronic structures.

Chemical modification is a promising method to deliver such changes to the surfaces. A number of reagents have been shown to be able to tether to TMDCs through covalent and non-covalent interactions [10,11]. For example, grafting of thiol-related compounds is a relatively well-explored method for the functionalization of MoS_2, which is an archetypal TMDC [12–14]. Iodomethane, iodoacetamide, and diazonium salts are other common small molecules that have been used for functionalization of TMDCs due to their ability to form a strong bond with the chalcogen atom [15–20]. However, chemical functionalization of TMDCs with diazonium salts does not proceed easily even when carried out on powdered samples [17,19]. For example, chemical exfoliation with organolithium reagents is often required to make MoS_2 accessible for nucleophilic attack and successful functionalization. Also, small flake sizes in powders (for example, only functionalized flakes that passed a 200 nm membrane were studied) [17] have prevented unambiguous identification of whether the functionalization occurred on edges, defects or basal planes.

Remarkably, $MoTe_2$ (an atomically thin cousin of MoS_2) appears to be more prone to functionalization without the need for a pre-treatment by organolithium reagents. Flakes (although of unspecified sizes) mechanically exfoliated from a single crystal of $MoTe_2$ have been reported to be passivated by diazonium chemistry [20], although it is unclear whether a covalent bond was formed upon grafting. Still, the ability of $MoTe_2$ to withstand aggressive electrophiles, such as 4-nitrobenzenediazonium tetrafluoroborate, without dissolution is remarkable, given the previous reports on the degradation of $MoTe_2$ under ambient conditions [10]. This suggests that $MoTe_2$ is a promising target for the functionalization chemistry and more research is needed in this direction. Since both

* Corresponding author.
** Corresponding author.
*** Corresponding author.
E-mail addresses: Guselnikovaoa@tpu.ru (O. Guselnikova), Alexey.Ganin@glasgow.ac.uk (A.Y. Ganin), postnikov@tpu.ru (P. Postnikov).

https://doi.org/10.1016/j.mtchem.2022.100846
2468-5194/

metallic and semiconducting polymorphs of $MoTe_2$ can be prepared as atomically-thin and continuous films [21] [–] [23] there are exciting opportunities for investigating the role of crystal structure of $MoTe_2$ on the reactivity with small molecules. The difference in the reactivity between MoS_2 and $MoTe_2$ suggests that alternative reagents could be explored for surface functionalization as well. Work in this direction could lead to new hybrid 2D materials as well as answering the question of whether a strong bond between $MoTe_2$ and grafting agent is formed.

Iodonium salts (ISs) are particularly interesting targets because unlike the commonly used diazonium salts, they manifest lower reduction potentials and a wider range of substituent functional groups (aromatic, alkynyl, alkyl, heterocyclic) that could be used for altering the chemical properties of the underlying TMDCs [24]. In addition, ISs are less prone to spontaneous reduction, making them very interesting targets for advanced control over surface grafting [25]. Furthermore, there are many ISs that have fluorine-containing groups, which could be used as markers for detection of whether the functionalization took place. For example, even minor quantities of F can be detected by XPS, making F-containing ISs well suited models for the mechanistic studies of reaction processes [26]. Finally, the ability of IS to be activated under stimuli (such as light [27], plasmonic resonance [28], chemical agents [29], and electric potential [30]) offers a better control over the reaction processes. Therefore, it is rather surprising that ISs have not been applied for chemical functionalization of TMDCs so far.

In this work, we demonstrate using $MoTe_2$ thin films that reaction with a symmetric bis(3,5-bis(trifluoromethyl)phenyl)iodonium salt results in surface functionalization of $MoTe_2$ with aryl-$(CF_3)_2$ groups as evidence by a comprehensive studies with Raman spectroscopy, XPS, AFM, and WCA. Remarkably, the reactive ability of the salts depends on the nature of the polymorphic phase used. This suggests that the electronic structure of the underlying $MoTe_2$ polymorph plays an important role in facilitating the reaction. In addition, the reaction of $MoTe_2$ with the iodonium salt provides an effective way of protecting (the otherwise unstable) $MoTe_2$ films against oxidation in ambient.

1. Results

1.1. Synthesis and characterization of $MoTe_2$ films

Thin films of the monoclinic 1T′- and hexagonal 2H–$MoTe_2$ were prepared in a CVD reactor at 650 °C using $FeTe_2$ precursor as the source of tellurium similar to previous work [22]. According to Raman spectroscopy the resulting products were either single-phased 1T′-$MoTe_2$ or 2H–$MoTe_2$ (Supplementary Fig. S1, Supplementary Table S1A) depending on the seeding layer used. The films were intentionally handled in air and no attempts were made to protect them from the ambient environment, for example, by encapsulation or deposition of a protective layer. AFM measurements (Supplementary Fig. S2) confirmed the film thicknesses of 8.2 ± 0.5 nm for 1T′-$MoTe_2$ (*ca.* 10 layers) and 9.4 ± 0.5 nm (*ca.*12 layers) for 2H–$MoTe_2$. XPS survey spectra (Supplementary Fig. S3) showed the presence of oxygen; while high-resolution XPS analysis of Mo 3d and Te 3d (Supplementary Fig. S4) showed the presence of oxidized states on the surface, typical for $MoTe_2$ films exposed to the ambient environment [31].

1.2. Reaction of 1T′-$MoTe_2$ films with bis(3,5-bis(trifluoromethyl) phenyl) iodonium salt (IS-CF_3)

Iodonium salts (ISs) are modification agents serving as the source of aryl radicals after the homolytic cleavage of the carbon–iodine bond (Fig. 1) [27]. In contrast to more widely explored aromatic diazonium salts, ISs may be advantageous due to the lower reduction potential, wider range of substituents, and broader range of stimuli that can be used for their activation [24,32]. As shown in Fig. 1, the carbon–iodine bond cleavage in ISs generates a radical that can attack the surface (which poses the question about the nature of the chemical bond created between $MoTe_2$ and aryl radicals), while the remaining fragment of the initial molecule is reduced to iodoarene that is not reactivated and can be easily removed by rinsing with solvent.

Bis(trifluoromethyl)phenyl)iodonium triflate (Supplementary Fig. S5) further denoted as **IS-CF_3**, was selected for the feasibility study of covalent functionalization of $MoTe_2$. After the reaction with the solvents was excluded (Supplementary Figs. S6–7), the 1T′-$MoTe_2$ film was immersed in a 1 mM solution of **IS-CF_3** in MeOH:CH_3CN for 1 h, repeatedly washed with degassed MeOH:CH_3CN, and finally dried under an argon flow. The initial analysis by Raman spectroscopy of the product (denoted as 1T′-$MoTe_2$-CF_3) showed a blue shift of the A_{1g} peak by 3 ± 1 cm^{-1} suggesting the functionalization took place (Fig. 2A, Supplementary Fig. S8 and Supplementary Table S1A). A similar shift of the A_{1g} mode, that represents out-of-plane vibrations, was previously observed in other chalcogenides (for example, upon reaction with electron-withdrawing molecules) [33,34] and can be explained by the difference in Ch–C and Ch–Mo (Ch = S, Se, Te) bond strengths [35]. On the other hand, the E^1_{2g} in-plane mode remains unaffected in terms of position and intensity (Supplementary Table S1A). E^1_{2g} is highly sensitive to interlayer interactions and because it remains unaffected, damage of the film after functionalization can be excluded [35]. Therefore, we concluded that grafting of aryl groups proceeded only to the top layer of $MoTe_2$ film.

XPS allows the detection of even minute amounts of fluorine [26], and thus the presence of CF_3 groups in **IS-CF_3** makes it an excellent functionalization marker (Supplementary Fig. S9). In addition, the F-peak at ≈690 eV in the survey XPS spectrum (Supplementary Fig. S10A) is well resolved and does not overlap with other peaks, for example, from $MoTe_2$ or the Si/SiO_2 substrate. According to the high-resolution spectrum, the appearance of F1s peak at 688.7 eV (with 1.7 at. % concentration) confirmed that the surface grafting with F-containing groups took place (Fig. 2B). The simple sorption of the salt on the surface or between $MoTe_2$ layers was excluded due to the absence of the I 3d peak (expected at BE = 622.9 and 634.4 eV). This suggested that decomposition of the salt followed by functionalization of the surface took place (Fig. 2C). In addition, the position of the peak at 292.6 eV in the high-resolution C 1s spectrum corresponded to the position of carbon in the CF_3 moiety (Fig. 2D). Finally, XPS mapping collected by scanning 121 points over the area of 1.5 × 1.6 mm^2 confirmed the lateral distribution of fluorine across the surface (Fig. 2G). The sum of the F1s signals obtained from the mapping experiments revealed a homogeneous distribution of fluorinated groups over the surface with the average spectrum centered at 688.7 eV and the intensities deviating only marginally (< 4%) from the average signal of 46,335 ± 1,726.8 cps (Supplementary Fig. S10B). The prolongation of functionalization time could lead to the increased content of F up to 4 at. % after 2.5 h of reaction (Fig. S10C). Based on the evidences collected we hypothesized that surface functionalization by 3,5-(trifluoromethyl)phenyl groups (further denoted as Ar-$(CF_3)_2$ for brevity) took place in a kinetically controlled manner.

In addition, significant changes observed in the high-resolution Mo 3d and Te 3d XPS spectra before and after the reaction with **IS-CF_3** seemed to confirm the hypothesis. First, there was a substantial decrease in the intensity of the peaks associated with Mo–O and Te–O bonds. This was evident from the change in the relative ratio of the peak intensities marked as Te–Mo/Te–O that changed from 1/1.02 to 1/0.06 (Fig. 2E). At the same time, the intensity ratio of

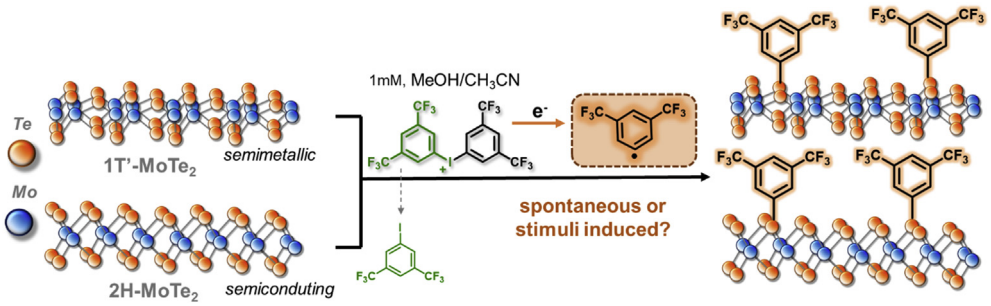

Fig. 1. Schematic illustration of 1T′- and 2H–$MoTe_2$ functionalization using iodonium salts. ISs decompose *via* C–I bond homolysis with the formation of aryl radicals that graft to the surface. The remaining iodoarene is removed by washing with solvent.

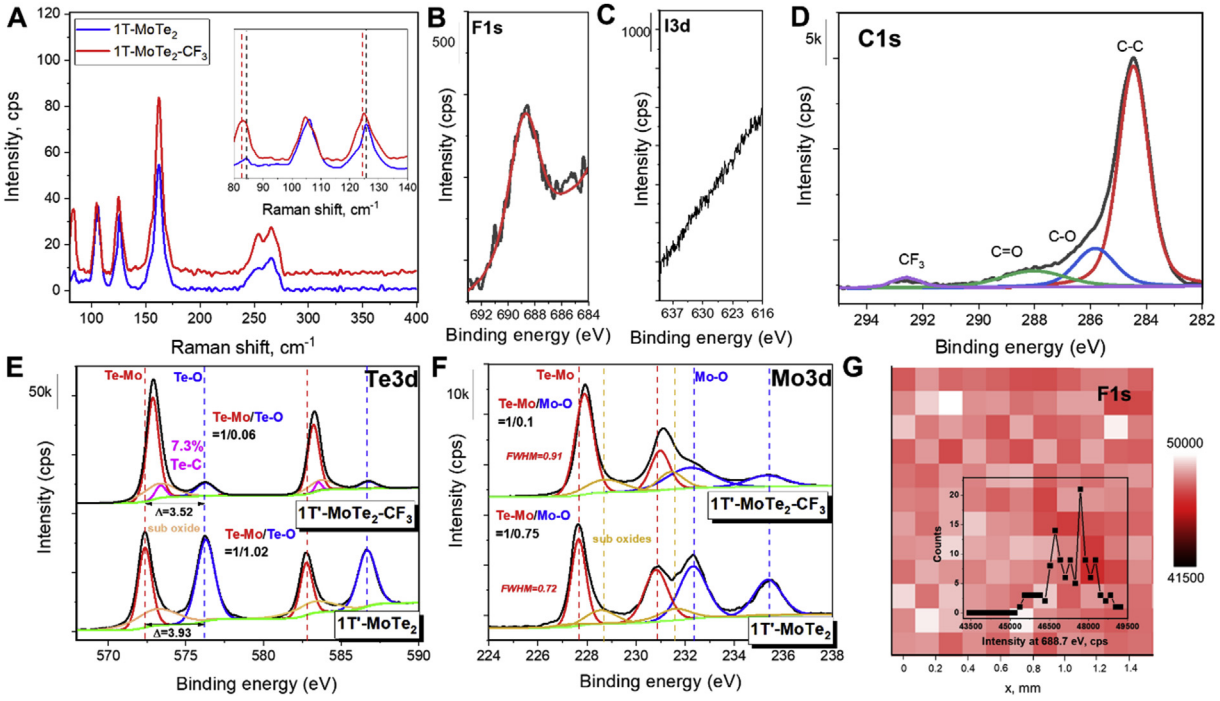

Fig. 2. The characterization of 1T′-$MoTe_2$ films before and after the treatment with bis(trifluoromethyl)phenyl)iodonium salt. The 633 nm Raman spectra of the film before (red line) and after (blue line) (**A**); High resolution XPS spectra corresponding to F 1s (**B**), I 3d (**C**), C 1s (**D**), Te3d (**E**), and Mo 3d regions (**F**). The XPS mapping of F 1s peak over the area of 1.5 × 1.6 mm^2. The insert shows distribution of intensities of the peaks from the F 1s mapping (**G**).

Mo–Te/Mo–O peaks decreased from 1/0.75 to 1/0.10, respectively (Fig. 2F). Secondly, the positions of Te 3d and Mo 3d peaks shifted by 0.4 eV and 0.15 eV, respectively (Supplementary Table S2). Thirdly, the full-width-at-half-maximum (FWHM) of Te $3d_{5/2}$ and Mo $3d_{5/2}$ peaks increased from 1.07 to 1.3 (Fig. 2E) and from 0.72 to 0.91, respectively (Fig. 2F). Similar peak shifts and broadening were observed in the Mo 3d XPS spectra of 1T-MoS_2 powders functionalized with aryl-iodides and diazonium salts [4,16–18].

Covalent functionalization could in principle proceed through the formation of O–C (from Mo–O and Te–O), Te–C, and Mo–C bonds. The significant reduction in the intensities of Mo–O, and Te–O probably excludes the formation of bonding with surface oxygen; otherwise, the functionalization would proceed without elimination of the oxide layer. The stronger shift of Te–Mo peaks by 0.40 eV *versus* Mo–Te peaks that shift by only 0.15 eV after the reaction with **IS-CF_3** suggests that Te-atoms are the probable binding sites for the functional moieties. In addition, the analogy with the functionalization chemistry of MoS_2, where the covalent bond is formed between chalcogen and carbon (rather than molybdenum and carbon), suggests that Te is a more likely binding site for covalent bond [4,18]. Furthermore, the broadening of Te $3d_{5/2}$ peaks at 572.8 eV (with the FWHM increasing from 1.07 to 1.3) suggests the presence of an additional component. This component is probably similar to the appearance of a prominent shoulder peak (ascribed to formation of covalent bond) in S 2p spectra of the functionalized MoS_2 [4,18]. Therefore, we deconvoluted the broadening of Mo–Te peak in the high-resolution Te 3d spectra of 1T′-$MoTe_2$-CF_3 into two components at BE = 573.37 ± 0.05 and 583.53 ± 0.05 eV (Fig. 2E). We ascribed the second component (pink trace in Fig. 2E) to the contibution from C–Te species. It was also possible to extract the information about the level of the functionalization in a similar fashion as it was carried previously for MoS_2 [18]. The relative degree of the covalent functionalization (calculated by dividing the peak area associated with this C–Te component to the total area of Te $3d_{5/2}$ peak) was found to be 7.3%.

In addition, the thickness of the organic layer at the surface was estimated from the Te 3d peak intensities using a method proposed previously with the relevant calculations given in the

Supplementary Note 1 [36]. Based on the observed attenuation of Te 3d spectra, the calculations revealed that Ar-$(CF_3)_2$ groups cover the surface with a density of 4.8×10^{14} molecules cm^{-2} while the thickness of the layer was found to be 1.3 ± 0.8 nm. These values are the same order of magnitude as those achieved on graphene functionalized with IS using an electrochemical process [37]. Considering the size of the Ar-$(CF_3)_2$ moieties 0.6 ± 0.2 nm, we can conclude that the formation of close to a monolayer coating is achieved [28]. The results are also close, for example, to previously observed coverages on gold surfaces [38].

To validate this assessment, we performed an AFM analysis across a 3×3 μm^2 area on 1T′-$MoTe_2$ before and after functionalization. The results showed a marginal increase in arithmetic deviations in surface roughness (R_a) from 0.73 ± 0.1 to 0.93 ± 0.1 nm that we attributed to the formation of a smooth thin organic layer (Supplementary Fig. S11). Remarkably, there is also a negligible change from 8.2 ± 0.5 to 8.5 ± 0.5 nm in the thickness of the film before and after reaction (Supplementary Fig. S11), again suggesting the formation of close to a monolayer film of grafted Ar-$(CF_3)_2$ moieties.

Given that the thickness of 1,3-bis(trifluoromethyl)phenyl monolayer $\approx 0.6 \pm 0.2$ nm is such a small value [27], the presence of a fluorinated aryl layer could also be determined by indirect experimental methods.

For example, if the functionalization takes place, it will lead to changes in the surface properties and increased hydrophobicity due to the presence of CF_3 groups. Respectively, the water contact angle (WCA) measurements showed that there was an increase in WCA from $76 \pm 2.1^\circ$ (similar to previously published results) [9] on the pristine film to $90 \pm 2.5^\circ$ after the reaction. The increase in WCA suggests the presence of hydrophobic fluorine-containing groups on the surface (Supplementary Fig. S12A) and further confirms that the grafting of functional groups takes place.

The functionalization of metallic $MoTe_2$ is expected to alter the electronic structure of 1T′ as electron extraction or injection depends on the dopant's/modification agent's electronegativity [16,35]. In the case of **IS-CF_3** it should lead to a *p*-type behavior due to the electron-withdrawing character of the CF_3 groups. Accordingly, the UV–vis measurements were carried out on 1T′-$MoTe_2$ films (deposited on quartz substrates) before and after functionalization. From the Tauc plots there is a change in the electronic properties of the films from initially metallic to a narrow bandgap semiconductor with $E_g \approx 0.3$ eV (Supplementary Fig. S12B).

Finally, we tested aromatic diazonium salts (ADSs) as a control modification agent for $MoTe_2$ thin films (Supplementary Note 2). Despite the fact that ADSs were reported as modification agents for $MoTe_2$ flakes obtained by mechanical exfoliation from a single crystal [20] we found that ADSs appeared to be unsuitable agents for the functionalization of the $MoTe_2$ films. According to Raman and XPS results (Supplementary Fig. S13) the 1T′-$MoTe_2$ film disintegrated after immersion into diazonium salt solution as no signals associated with $MoTe_2$ were detected by Raman and XPS Mo 3d and Te 3d spectroscopy. Therefore, the functionalization of 1T′-$MoTe_2$ by **IS-CF_3** offers a more controllable route because it does not seem to compromise the integrity of the film.

1.3. Light-induced reaction of 2H–$MoTe_2$ films with bis(3,5-bis(trifluoromethyl)phenyl)iodonium salt

Inspired by the successful spontaneous functionalization of 1T′-$MoTe_2$ films by **IS-CF3**, identical experiments were carried on 2H–$MoTe_2$. As before, a fully characterized 2H–$MoTe_2$ film was immersed in 1 mM solution of **IS-CF_3** in MeOH:CH_3CN for 1 h, repeatedly washed with dry MeOH:CH_3CN and finally dried under an argon flow. However, the XPS survey spectrum of the resulting film showed the presence of 0.3 at. % of iodine along with 0.9 at. % of fluorine (Supplementary Fig. S14) which suggested the sorption of the salt instead of covalent functionalization as was the case for 1T′-$MoTe_2$. The I 3d signal was still observed on 2H–$MoTe_2$ after extensive washing (identical experimental procedure as for 1T′-$MoTe_2$) confirming stronger interaction of **IS-CF_3** with the formation of surface complex. Notably, the high-resolution I 3d spectrum (Supplementary Fig. S14) obtained after reaction between 2H–$MoTe_2$ and **IS-CF_3** displayed two peaks unlike the I 3d spectrum of pristine **IS-CF_3** powder (Supplementary Fig. S9). This suggested a formation of a surface complex due to an electrostatic interaction with the surface [9]. However, an additional assessment by WCA method, showed (within the experimental error of 2–3°) that there was no substantial wettability change (Supplementary Fig. S15). Therefore, we concluded that the **IS-CF_3** molecules were physically adsorbed at the surface.

However, the low reactivity of **IS-CF_3** towards 2H–$MoTe_2$ is expected because the activation of ISs commonly proceeds through the cleavage of the C–I bond (Fig. 1). To cleave the bond an additional stimulus (such as applied potential or exposure to light) is required before surface grafting even takes place [24,26,28,29,39]. Light is a mild-stimuli and it is often used in surface modification [27,40]. Therefore, we hypothesized that semiconducting 2H–$MoTe_2$ with a band gap of $E_g \approx 1.1$ eV would generate high-energy state electron–hole pairs upon illumination with photon energy higher than the E_g (Supplementary Fig. S16). The presence of the pairs could provide a pathway for the excitation of the surface complexes with the formation of dissociative states [26,41].

To test this hypothesis, we performed the reaction of 2H–$MoTe_2$ with **IS-CF_3** under illumination of an LED with 780 nm wavelength (1.6 eV). The XPS analysis of the sample revealed the disappearance of I 3d peaks (Fig. 3A) while the F-content (from F 1s XPS) was detected at 2.1 at. % (Fig. 3B, Supplementary Fig. S17). The peak in C 1s spectra associated with CF_3 groups at 292.38 eV was also observed (Fig. 3C). Therefore, we concluded that the photon energy (corresponding to wavelength of 780 nm) was sufficient to initiate the decomposition of **IS-CF_3** due to the photoexcitation of electrons in semiconducting 2H–$MoTe_2$. Experiments under illumination with a lower energy light source were also carried out as described in Supplementary Note 3 and Supplementary Fig. S18.

The 633 and 523 nm Raman spectra on the functionalized film revealed that the positions and intensities of E_{12g} peaks remained unchanged (Fig. 3D, Supplementary Fig. S19, Supplementary Table S1B). However, there is a blue shift of 3 ± 1 cm^{-1} for A_{1g} vibration modes after the LED driven reaction with **IS-CF_3** [35]. In addition, the XPS data shows that Te–Mo peaks shift by 0.40 eV (Mo–Te shifts only by 0.15 eV) compared to the pristine film (Fig. 3E). There is also a broadening of the Te 3d peaks after the reaction (FWHM increased from 1.1 to 1.3 eV) suggesting the appearance of a new component in the same way as was described above for the functionalized 1T′-$MoTe_2$ films. Thus, the grafting of Ar-$(CF_3)_2$ groups in 2H–$MoTe_2$ probably proceeds through Te sites with the formation of a covalent Te–C bond (Fig. 3E). The degree of covalent functionalization (functional groups per Te), calculated based on the peak area underneath of this C–Te component relative to the total area of Te 3d, was found to be 11.8% which was higher than for 1T′-$MoTe_2$.

However, even though the intensities of the peaks associated with Te–O/Mo–O bonds in high resolution Mo 3d and Te 3d XPS spectra are significantly suppressed in the functionalized 2H–$MoTe_2$ film (Fig. 3E,F) they are more pronounced than in case of the functionalized 1T′-$MoTe_2$ film (Fig. 2E,F). This indicates a higher oxygen content in the functionalized 2H–$MoTe_2$ films compared to the functionalized 1T′-$MoTe_2$ films. This may explain that, in comparison with the 1T′-$MoTe_2$ films, the reaction of **IS-CF_3** with

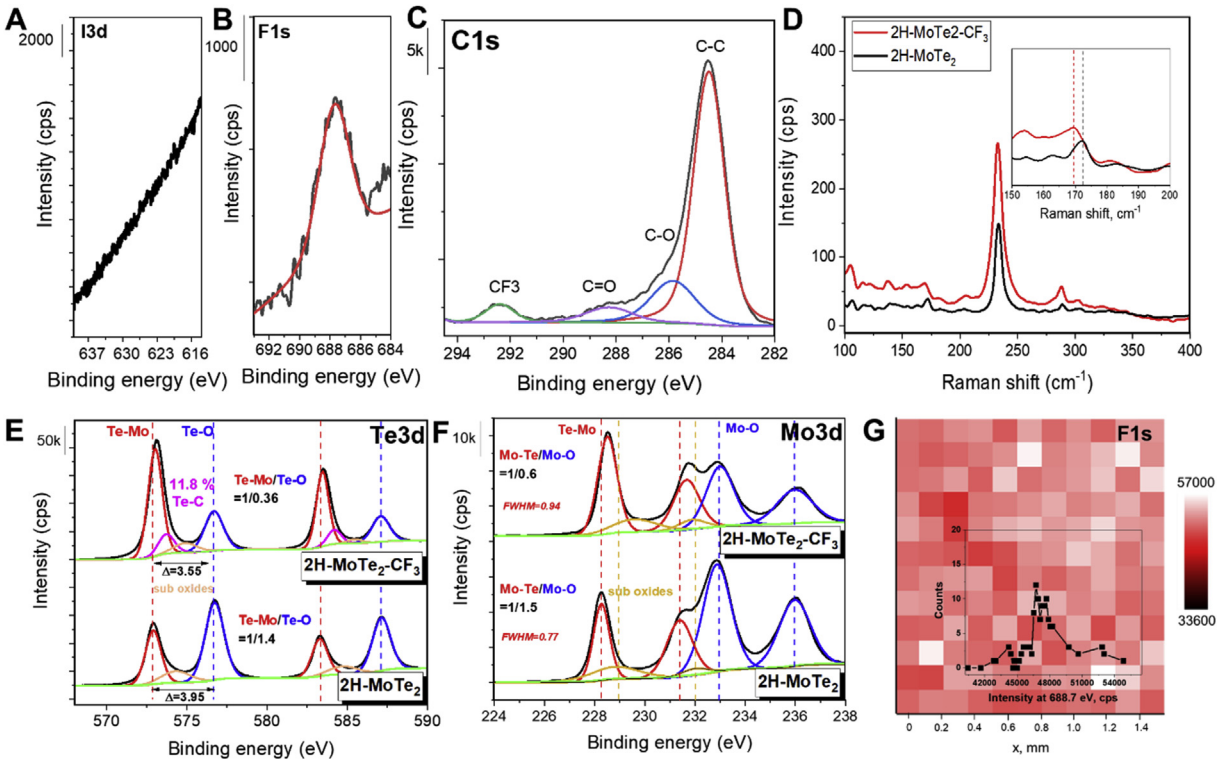

Fig. 3. Surface chemical composition of 2H−$MoTe_2$ before and after spontaneous treatment with **IS-CF_3**. High resolution XPS spectra of I 3d (**A**), F 1s (**B**), C 1s (**C**), Te 3d (**E**), and Mo 3d (**F**); Raman spectra of 2H−$MoTe_2$ and 2H-$MoTe_2$-IS-CF_3 (**D**); The XPS mapping of F 1s peak over the area of 1.5 × 1.6 mm^2. The insert shows distribution of intensities from XPS F1s mapping (**G**).

2H−$MoTe_2$ led to a less homogeneous distribution of the organic layer according to the XPS mapping. The mapping showed the broader distribution of intensities of F 1s peak across the scanned area (Fig. 3G, Supplementary Fig. S19B) with the average spectrum centered at 688.7 eV and the intensities deviating moderately (< 6.6%) from the average signal of 46,655.2 ± 3,111.3 cps. We hypothesize that upon light illumination of 2H−$MoTe_2$, the same reaction with **IS-CF_3** as for 1T-$MoTe_2$ takes place: selective C−I bond cleavage followed by the covalent functionalization of 2H−$MoTe_2$ over Te-sites by generated aryl radicals. However, due to the more pronounced peaks associated with Te−O/Mo−O the attachment of Ar-$(CF_3)_2$ groups may proceed through the O-sites as well. This could be explained by the fact that upon intense light illumination more active organic radicals are generated and these may have propensity to react with the oxidized layer [42].

The AFM measurements showed that in comparison with 1T′-phase there is a larger increase in surface roughness upon functionalization as well. The increase of R_a values from 0.69 ± 0.1 nm (before, Supplementary Fig. S20A) to 1.2 ± 0.1 nm (after, Supplementary Fig. S20B) suggests that there might be locations of the film with different degrees of functionalization. Also, the difference between the film's thickness (1.6 ± 0.5 nm, given the thickness of 1,3-bis(trifluoromethyl)phenyl monolayer, Supplementary Fig. S20C) before and after functionalization is larger according to AFM data and XPS (2.1 ± 0.8 nm, Supplementary Note 1). This suggests the formation of a thicker (or possibly more inhomogeneous) organic ad-layer on 2H−$MoTe_2$ films compared with 1T′-$MoTe_2$. Therefore, we can't exclude the possibility of formation of bilayer structure on 2H−$MoTe_2$ film. Although 3,5-bis(trifluoromethyl)phenyl groups provide the steric hindrance for the multilayer growth, the fourth position in the aromatic ring is still available for further attack under additional stimuli (Fig. S20D) as was shown for diazonium functionalization [43].

Still, as shown by WCA studies (Supplementary Fig. S21A), the surface of the functionalized 2H−$MoTe_2$ is hydrophobic (WCA increased from 70° to 95°). Such hydrophobic behavior confirms the functionalization with a conformation of molecules orthogonal to the surface. The UV−Vis spectroscopy and corresponding Tauc plots (Supplementary Fig. S21B), suggest that the semiconducting properties [3,44] of 2H−$MoTe_2$ are preserved with only a minor bandgap change from E_g = 1.12 eV to E_g = 1.13 eV after functionalization.

The formation of an Ar-$(CF_3)_2$ layer in both 1T′- and 2H-phases provides exciting opportunities for resolving the long-standing challenge of oxidation of $MoTe_2$ (and some 2D materials in general) in ambient conditions [45,46]. The protection strategies for $MoTe_2$ thin films from air exposure commonly rely on encapsulation by boron nitride [47] and graphene [23]. The growth of protective layer of Al_2O_3 has been also reported [48]. The simplicity of the covalent functionalization is a promising strategy because it proceeds through the removal of the oxide layer and therefore, it could be applied on films previously exposed to the ambient.

1.4. The stability of $MoTe_2$ films functionalized by IS-CF_3

The impact of the reaction with **IS-CF_3** on the films' stability towards ambient conditions was investigated by exposing the as-prepared and functionalized films to moist air and direct sunlight for 336 h. As mentioned above, the as-prepared 1T′-$MoTe_2$ and 2H-films were handled in air and had a significant amount of surface oxides even before the stability experiments. However, from the comparison of the high-resolution Mo 3d and Te 3d XPS spectra, the degradation of the non-functionalized films continued after exposure to the ambient. In the non-functionalized 2H−$MoTe_2$ the intensity ratio between Mo−Te/Mo−O peaks changed from 1/1.5–1/5.3 and for Te−Mo/Te−O from 1/1.5–1/8.3, revealing that

continuous surface oxidation, especially on tellurium sites, takes place over time (Fig. 4A). Similar ratios were registered for 1T′-$MoTe_2$ films as well (Fig. 4B). The films experienced a significant degradation in line with previous reports showing the rapid degradation of $MoTe_2$ films in ambient conditions [46]. It has been also reported that the Mo–Te–O layer growth does not seem to stop but proceeds (although slowly) until complete degradation of the film. This may be less of an issue with few-layered films studied in this work, but it would certainly present a significant challenge for mono- or bi-layer $MoTe_2$ films that are important in technological applications.

However, as evident from the high-resolution Te 3d and Mo 3d spectra recorded on functionalized 1T′- and 2H–$MoTe_2$ films before and after the 336 h of the stability experiment, the Mo–Te/Mo–O and Te–Mo/Te–O peak ratios remain constant (Fig. 4A,B). We hypothesize that the stability of functionalized $MoTe_2$ is explained by the covalent attachment of Ar-$(CF_3)_2$ groups over Te-sites and the hydrophobic nature of CF_3 groups that repel moisture. Hence, the reaction with **IS-CF_3** provides a simple and efficient way for protecting films from the ambient conditions, broadening the possibilities for future applications of $MoTe_2$.

Remarkably, despite XPS points out continuous oxidation, the as-made, non-functionalized films still show the characteristic peaks of 1T′-$MoTe_2$ or 2H–$MoTe_2$ in the Raman spectra (Supplementary Fig. S22). This suggests that, unlike XPS, Raman spectroscopy provides only qualitative assessment of the films and does not detect oxide phases. However, the change in characteristic Raman peak intensities at 125.7 cm^{-1} (1T′-$MoTe_2$) and 230.1 cm^{-1} (2H–$MoTe_2$) relative to the intensity of the silicon peak at 520.1 cm^{-1} can be used to monitor the degradation with time (Supplementary Fig. S22). While in non-functionalized $MoTe_2$ films the relative intensity ratios reduced by half after 336 h of exposure to ambient conditions, in the functionalized $MoTe_2$ they remained constant (Fig. 4C).

Finally, while the WCA measured on pristine, non-functionalized 1T′- and 2H–$MoTe_2$ after 336 h of stability measurements decreased, the WCA of the functionalized film remained unchanged in line with the hydrophobic nature of the surface due to the attachment of Ar-$(CF_3)_2$ groups (Fig. 4D). Interestingly, the damaging effect of moisture is visually evident from the appearance of the 2H–$MoTe_2$ surface after WCA measurements: traces from water drops with lighter colors are well-visible (Supplementary Fig. S23). The XPS analysis from the regions demonstrated the increased oxidation of the surface (Supplementary Fig. S24). In contrast to pristine 2H–$MoTe_2$, the surface of functionalized 2H–$MoTe_2$ remains the same after contact with water suggesting protection against moisture is achieved due to a lower interaction with water molecules. Overall, the experiments provided convincing evidences that covalent functionalization with Ar-$(CF_3)_2$ took place and further mechanistic insights into the process are needed. Alternative methods of protection against oxidation such as BN, Al_2O_3 etc [47,48] are quite expensive and challenging to perform. In contrast to them, the developed in this work functionalization procedure is more accessible in terms of

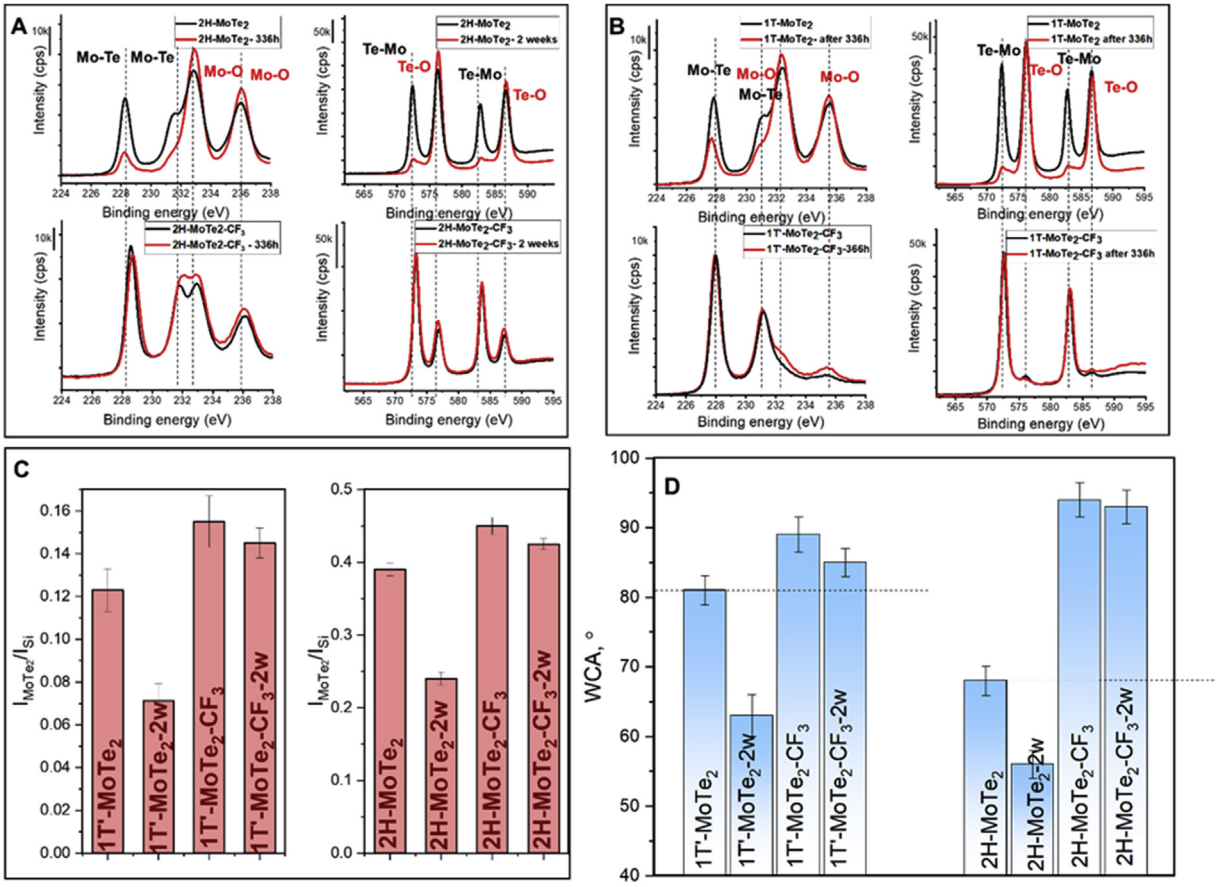

Fig. 4. Protective properties of functionalized $MoTe_2$-CF_3 compared to pristine $MoTe_2$.High resolution XPS spectra from Mo 3d and Te 3d regions for 2H/1T′-$MoTe_2$ and 2H/1T′-$MoTe_2$–CF_3 (**A, B**); comparison of characteristic Raman peak ratios I_{MoTe2}/I_{Si} after 336 h in air (**C**) and WCA measurement data (**D**).

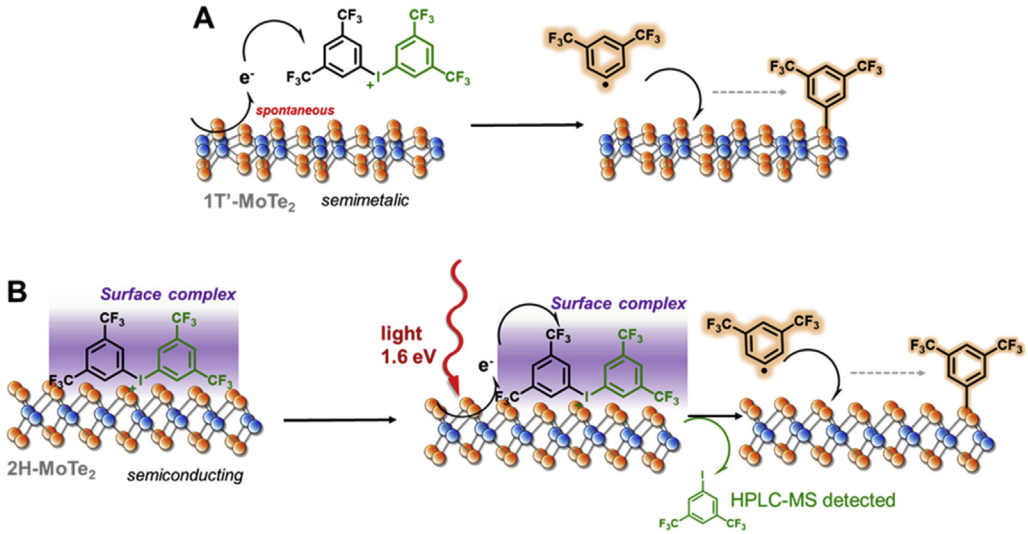

Fig. 5. Proposed mechanism of the functionalization of 1T'- (**A**) and 2H−$MoTe_2$ (**B**) thin films with **IS-CF_3**.

equipment and chemicals. However, the observed changes in the electronic structure of $MoTe_2$ films (Figs. S12 and S21) after functionalization should be considered as well.

1.5. Mechanistic insight into $MoTe_2$ functionalization using ISs

The functionalization of various surfaces by ISs has been described as occurring *via* a two-step process [28–30,39]. Firstly, the cleavage of C–I bond takes place after interaction with the substrate, often with additional stimuli (electric potential, light, plasmon). The bond cleavage leads to the generation of an aryl radical and iodobenzene (Fig. 5). Secondly, the generated radicals attacks the surface with the formation of a new bond, while iodobenzene remains in solution.

Based on the evidence from XPS, Raman spectroscopy, AFM, WCA, as well as stability of the functionalized films presented above, we hypothesized that the electron transfer from $MoTe_2$ was a major factor for the radical generation that reacts with Te sites. This hypothesis is consistent with the reaction mechanism reported for other semiconducting surfaces, for example, F-doped indium tin oxide [49]. To test this hypothesis and find out whether the radical pathway for $MoTe_2$ takes place, we first investigated whether 3,5-(trifluoromethyl)iodobenzene was formed as a byproduct. HPLC-MS data (Supplementary Fig. S25) confirmed the presence of 3,5-(trifluoromethyl)iodobenzene and thus, provided direct evidence that **IS-CF_3** underwent radical decomposition.

In addition, we utilized the common radical scavenger (2,2,6,6-Tetramethylpiperidin-1-yl)oxyl (TEMPO), which was added equimolarly together with **IS-CF_3** during the reaction. TEMPO can quench the generated aryl radicals. That means if the reaction takes place over radical formation, then the presence of TEMPO would prevent the functionalization of the surface by entrapping of the reactive species (Supplementary Fig. S26A). In line with this assessment, in the presence of TEMPO, the high-resolution F 1s is absent from the XPS spectrum (Supplementary Fig. S26B). Similarly, the peak related to CF_3 is absent from the C 1s spectrum (Supplementary Fig. S26C). This suggests that aryl radical generated during the reaction process were trapped by TEMPO and thus, prevented them from reacting with the $MoTe_2$ surface. These collective results confirm the radical nature of the $MoTe_2$ functionalization process.

The detailed study of the interaction of metallic 1T′-$MoTe_2$ and semiconducting 2H−$MoTe_2$ with **IS-CF_3** revealed different reactivity of the polymorphs with the generated radical, which can be explained by the difference in the electronic structures of the polymorphs. From the electronic point of view, the 1T′-phase is a metal with a significant number of delocalized electrons available for metallic transport behavior [50]. Therefore, the absence of band gap enables the transfer of electrons to the **IS-CF_3** molecule. This triggers the generation of radicals and results in spontaneous grafting of Ar-$(CF_3)_2$ as shown in Fig. 5A. However, light illumination is required for semiconducting 2H−$MoTe_2$ to generate electron transfer as there is no spontaneous electron transfer to IS. Therefore, **IS-CF_3** forms a charge-transfer complex at the 2H−$MoTe_2$ surface (Fig. 5B). The surface complex enables the cleavage of C–I bond. The cleavage is accelerated by electron transfer due to the energy provided by illumination with a photon energy is larger than the 2H−$MoTe_2$ energy bandgap [41]. Similar reactivity patterns were proposed for MoS_2 [13] and single-walled carbon nanotubes, where the metallic CNTs were found to be more reactive towards diazonium salts than semiconducting ones [51]. The specificity for stimuli offers exciting directions for adapting the strategy to other TMDCs, where reactivity may be dictated by electronic structure. Moreover, laser illumination opens perspectives for selective functionalization reversal as previously shown for the case of graphene with diazonium salts [52].

2. Conclusions

In conclusion, we provide the first example of successful covalent functionalization of $MoTe_2$ by a symmetrical iodonium salt. A detailed XPS study shows that functional 3,5-bis(trifluoromethyl) phenyl groups are grafted directly onto the surface suggesting the formation of covalent Te–C bonds. The utility of **IS-CF_3** as a reagent demonstrates that the grafting of the organic layer prevents atomically thin films of $MoTe_2$ from further oxidation. This is evidenced by the lack of noticeable changes in WCA, Raman and XPS spectra over the period of at least 2 weeks confirming the protecting function of 3,5-bis(trifluoromethyl)phenyl groups. Thus, the proposed method offers a practical solution to a long-standing challenge associated with the spontaneous oxidation of $MoTe_2$.

A strong impact on the future direction in device fabrication as well as finding (and preserving) new electronic states in exotic (but unstable in ambient) 2D materials could be anticipated. Moreover, as the reactivity of **IS-CF_3** depends on the electronic structure of the 1T′-$MoTe_2$ and 2H−$MoTe_2$ polymorphs, the reported functionalization strategy may open new ways for a targeted functionalization

of 2D materials. For example, **IS-CF_3** reacts spontaneously through C—I bond cleavage with the metallic 1T′-$MoTe_2$. In contrast, the semiconducting 2H—$MoTe_2$ forms a surface complex with **IS-CF_3**, which decomposes under light exposure with a photon energy larger than the band gap of 2H—$MoTe_2$. This could potentially provide a platform for the precise modification of thin films, for example, by the attenuation of homojunctions between two polymorphic $MoTe_2$ phases.

Finally, functionalization with iodonium salts opens new directions in the selective tuning of the chemical properties of $MoTe_2$, for example, by changing the nature of the substitution groups in the grafted aryl molecule or aliphatic/heterocyclic groups. This could be then extended to TMDCs and other 2D materials, where reactivity is dictated by the electronic states, providing exciting opportunities for their fundamental science and applications.

3. Methods

300 nm SiO_2/Si (100) (Inseto) substrates (10 × 10 mm^2) were first cleaned by sonication in acetone for 10 min, followed by sonication in isopropyl alcohol for a further 10 min before being dried under a stream of nitrogen gas. Molybdenum (99.95%) precursor films were deposited on to the cleaned 300 nm SiO_2/Si substrates via electron beam physical vapor deposition using a Plassys MEB550s. Deposition occurred under a vacuum of 1×10^{-6} mbar at a rate of 0.07 nm/s, with the electron beam gun emission current at 220 mA. Molybdenum trioxide precursor films were deposited on to the cleaned 300 nm SiO_2/Si substrates by thermal evaporation of MoO_3 pellets (99.99%, Pi-Kem) in a Plassys MEB400 under a vacuum of 2×10^{-6} mbar at a rate of 0.2 nm/s. The precursor films were then converted into 2H- and 1T′-$MoTe_2$ by CVD with the nature of the precursor layer dictating the phase of $MoTe_2$ as described in previously published work [22]. The substrate with precursor layer was placed in the hot zone of a horizontal Lenton tube furnace with the $FeTe_2$ source (30 mg) positioned 7 cm upstream. The dwell temperature of the source and substrate were set at 630 and 650 °C, respectively. The dwell temperatures were reached at a ramp rate of 5 °C/min with dwell time of 4 h before cooling naturally to room temperature. Throughout the deposition process, a carrier gas of 5% H_2/Ar was flowed through the CVD chamber at a rate of 300 sccm. Before beginning the deposition process the chamber was evacuated to a pressure of 1×10^{-2} mbar and subsequently refilled with the carrier gas, this was repeated for a total of three cycles to ensure an oxygen free environment for the deposition.

Methanol (MeOH) and acetonitrile (MeCN) were purchased from Sigma—Aldrich and degassed by freeze—pump—thaw (3 cycles) followed by purging the solvent with Ar for at least 30 min. $MoTe_2$ films were immersed in 5 ml of freshly prepared 1 mM bis(3,5-bis(trifluoromethyl)phenyl)iodonium trifluoromethanesulfonate or 3,5-bis(trifluoromethyl)benzenediazonium tosylate (see Supplementary information for synthesis) solutions in MeOH/CH_3CN (1/1 vv) and kept for 1 h without stirring. After, samples were removed and washed by immersion in MeOH for 45 min 3 times and dried under Ar flow. For experiment under LED irradiation $MoTe_2$ films were immersed in 5 mL of freshly prepared 1 mM bis(3,5-bis(trifluoromethyl)phenyl)iodonium trifluoromethanesulfonate or 3,5-bis(trifluoromethyl)benzenediazonium tosylate in a petri dish and coated with transparent glass cover. They were irradiated by LED sources (1,050 nm, 50 mW Thorlab product number M1050L4 or 780 nm, 800 mW, (Thorlab product number M780LP1) from 1 cm distance for 1 h and washed by immersion in MeOH for 45 min 3 times and dried under Ar flow.

X-ray photoelectron spectroscopy (XPS) was performed on S-Probe monochromatized XPS spectrometer (Thermo-scientific XPS NEXSA) with AlKα x-ray (1,486.6 eV) monochromatic source (take off angle: θ = 90°; voltage and power of the source 10 kV, 200 W. A flood gun was used for compensation of charging effects. The XPS survey spectra were collected with a pass energy Ep = 157.7 eV and energy steps Es = 0.22 eV, the high-resolution spectra with Ep = 107.5 eV and Es = 0.1 eV. The XPS spectra were analyzed using Avantage software. High resolution envelopes were fitted using Smart baseline method.

Raman spectroscopy was performed using a thermo scientific iXR Raman spectrometer with a 532 nm laser set at 1 mW with an acquisition time of 40 s per scan. The Raman spectra obtained under 633 nm laser excitation were recorded in the backscattering geometry in a confocal Raman microscope (NT-MDT Spectral Instruments, Russia), with the laser beam focused on the sample with a 100x objective. Thirty spectra were averaged at 1 s per spectrum.

Atomic force microscopy was performed in the semi-contact mode using a scanning probe microscope (NT-MDT, The Netherlands). The images were background subtracted and used for roughness and film thickness determination at the same $MoTe_2$/SiO_2 location before and after functionalization. The reported film thicknesses are the means of at least 5 values obtained from three scratches, and the uncertainty is the standard deviation of the mean value.

The water contact angle (WCA) was evaluated using a Drop Shape Analyzer—DSA25 (Kruss, Germany) at 10 positions (drop volume - 2 μL) at room temperature. The sessile drop method in air was used during WCA measurements. The measurements were processed using the software package ADVANCE (Kruss, Germany).

The Agilent Technologies 1,290 Infinity II series HPLC system was used for chromatography measurements using a column Zorbax Eclipse Plus C18 column (50 mm × 2.1 mm, 1.8 μm, Agilent, USA) at 40 °C temperature with a flow rate of 0.3 ml/min and isocratic consisting of mobile phase acetonitrile (A) and 0.1% trifluoroacetic acid in water (B) at the ratio 1:1. Injection volume was 10 μL and temperature with autosampler temperature 10 °C.

For the tandem mass spectrometric (MS/MS) analysis, an Agilent 6,470 triple quadrupole LC/MS spectrometer (QQQ) (Agilent Technologies, USA) equipped with an electrospray ionization source (ESI) operating in positive mode was used. The operating parameters were the following: drying gas (nitrogen), temperature 350 °C with a flow rate of 8 L/min, nebulizer gas (nitrogen) 40 psi, capillary voltage 3,500 V. The MS/MS detector was run in the multiple reaction monitoring (MRM) mode. The optimal parameters of MRM analysis were mass transitions 341 → 75, fragmentor voltage 135 V and collision energy (CE) 35 eV.

The UV—Vis spectra were measured using spectrometer Lambda 25 (Perkin—Elmer) in 200—1,100 nm wavelength range using $MoTe_2$ film prepared on quartz substrates.

Author contributions

OG, AYG, and PP conceived and managed the experiments. OG designed the experiments and carried them out with the help of NS and ES. OG analyzed and plotted the data. RR carried out AFM and Raman measurements. AI carried out LC-MS experiments. OG and AYG wrote the manuscript. JF designed and carried out CVD experiments. All authors have contributed to writing of the manuscript and have given approval to the final version of the manuscript.

Data availability

The raw data required to reproduce these findings are available on request to corresponding authors.

Declaration of competing interest

The authors declare that they have no known competing financial interests or personal relationships that could have appeared to influence the work reported in this article.

Acknowledgements

This work was supported by the Russian Science Foundation (RSF-17-73-20066). AYG and JPF acknowledge EPSRC (EP/N509668/1) for supporting their work.

Appendix A. Supplementary data

Supplementary data to this article can be found online at https://doi.org/10.1016/j.mtchem.2022.100846.

References

[1] Y. Chen, Z. Fan, Z. Zhang, W. Niu, C. Li, N. Yang, B. Chen, H. Zhang, Two-dimensional metal nanomaterials: synthesis, properties, and applications, Chem. Rev. 118 (2018) 6409–6455, https://doi.org/10.1021/acs.chemrev.7b00727.
[2] S. Manzeli, D. Ovchinnikov, D. Pasquier, O.V. Yazyev, A. Kis, 2D transition metal dichalcogenides, Nat. Rev. Mater. 2 (2017) 17033, https://doi.org/10.1038/natrevmats.2017.33.
[3] L. Reeves, Y. Wang, T.F. Krauss, 2D material microcavity light emitters: to lase or not to lase? Adv. Opt. Mater. 6 (2018) 1800272, https://doi.org/10.1002/adom.201800272.
[4] E.E. Benson, H. Zhang, S.A. Schuman, S.U. Nanayakkara, N.D. Bronstein, S. Ferrere, J.L. Blackburn, E.M. Miller, Balancing the hydrogen evolution reaction, surface energetics, and stability of metallic MoS2 nanosheets via covalent functionalization, J. Am. Chem. Soc. 140 (2018) 441–450, https://doi.org/10.1021/jacs.7b11242.
[5] J.C. McGlynn, T. Dankwort, L. Kienle, N.A.G. Bandeira, J.P. Fraser, E.K. Gibson, I. Cascallana-Matías, K. Kamarás, M.D. Symes, H.N. Miras, A.Y. Ganin, The rapid electrochemical activation of MoTe2 for the hydrogen evolution reaction, Nat. Commun. 10 (2019) 1–9, https://doi.org/10.1038/s41467-019-12831-0.
[6] J. Yang, A.R. Mohmad, Y. Wang, R. Fullon, X. Song, F. Zhao, I. Bozkurt, M. Augustin, E.J.G. Santos, H.S. Shin, W. Zhang, D. Voiry, H.Y. Jeong, M. Chhowalla, Ultrahigh-current-density niobium disulfide catalysts for hydrogen evolution, Nat. Mater. 18 (2019) 1309–1314, https://doi.org/10.1038/s41563-019-0463-8.
[7] M. Liu, H. Zhu, Y. Wang, C. Sevencan, B.L. Li, Functionalized MoS2-based nanomaterials for cancer phototherapy and other biomedical applications, ACS Mater. Lett. 3 (2021) 462–496, https://doi.org/10.1021/acsmaterialslett.1c00073.
[8] P. Karthick Kannan, P. Shankar, C. Blackman, C. Chung, Recent advances in 2D inorganic nanomaterials for SERS sensing, Adv. Mater. 31 (2019) 1803432, https://doi.org/10.1002/adma.201803432.
[9] J. Fraser, P.S. Postnikov, E. Miliutina, Z. Kolska, R. Valiev, V. Švorčík, O. Lyutakov, A.Y. Ganin, O. Guselnikova, Application of a 2D molybdenum telluride in SERS-detection of biorelevant molecules, ACS Appl. Mater. Interfaces 15 (2020) 54, https://doi.org/10.1021/acsami.0c11231.
[10] X. Chen, A.R. McDonald, Functionalization of two-dimensional transition-metal dichalcogenides, Adv. Mater. 28 (2016) 5738–5746, https://doi.org/10.1002/adma.201505345.
[11] L. Daukiya, J. Seibel, S. De Feyter, Chemical modification of 2D materials using molecules and assemblies of molecules, Adv. Phys. X. 4 (2019) 1625723, https://doi.org/10.1080/23746149.2019.1625723.
[12] X. Chen, N.C. Berner, C. Backes, G.S. Duesberg, A.R. McDonald, Functionalization of two-dimensional MoS2: on the reaction between MoS2 and organic thiols, Angew. Chem. Int. Ed. 55 (2016) 5803–5808, https://doi.org/10.1002/anie.201510219.
[13] M. Morant-Giner, J.M. Carbonell-Vilar, M. Viciano-Chumillas, A. Forment-Aliaga, J. Cano, E. Coronado, Functionalisation of MoS2 2D layers with diarylethene molecules, J. Mater. Chem. C. 9 (2021) 10975–10984, https://doi.org/10.1039/D1TC01133B.
[14] Q. Li, Y. Zhao, C. Ling, S. Yuan, Q. Chen, J. Wang, Towards a comprehensive understanding of the reaction mechanisms between defective MoS2 and thiol molecules, Angew. Chem. Int. Ed. 56 (2017) 10501–10505, https://doi.org/10.1002/anie.201706038.
[15] X.S. Chu, A. Yousaf, D.O. Li, A.A. Tang, A. Debnath, D. Ma, A.A. Green, E.J.G. Santos, Q.H. Wang, Direct covalent chemical functionalization of unmodified two-dimensional molybdenum disulfide, Chem. Mater. 30 (2018) 2112–2128, https://doi.org/10.1021/acs.chemmater.8b00173.
[16] D. Voiry, A. Goswami, R. Kappera, C.D.C.C.E. Silva, D. Kaplan, T. Fujita, M. Chen, T. Asefa, M. Chhowalla, Covalent functionalization of monolayered transition metal dichalcogenides by phase engineering, Nat. Chem. 7 (2015) 45–49, https://doi.org/10.1038/nchem.2108.
[17] K.C. Knirsch, N.C. Berner, H.C. Nerl, C.S. Cucinotta, Z. Gholamvand, N. McEvoy, Z. Wang, I. Abramovic, P. Vecera, M. Halik, S. Sanvito, G.S. Duesberg, V. Nicolosi, F. Hauke, A. Hirsch, J.N. Coleman, C. Backes, Basal-plane functionalization of chemically exfoliated molybdenum disulfide by diazonium salts, ACS Nano 9 (2015) 6018–6030, https://doi.org/10.1021/acsnano.5b00965.
[18] X. Chen, C. Bartlam, V. Lloret, N. Moses Badlyan, S. Wolff, R. Gillen, T. Stimpel-Lindner, J. Maultzsch, G.S. Duesberg, K.C. Knirsch, A. Hirsch, Covalent bis-functionalization of two-dimensional molybdenum disulfide, Angew. Chem. Int. Ed. 60 (2021) 13484–13492, https://doi.org/10.1002/anie.202103353.
[19] L. Daukiya, J. Teyssandier, S. Eyley, S. El Kazzi, M.C. Rodríguez González, B. Pradhan, W. Thielemans, J. Hofkens, S. De Feyter, Covalent functionalization of molybdenum disulfide by chemically activated diazonium salts, Nanoscale 13 (2021) 2972–2981, https://doi.org/10.1039/D0NR07310E.
[20] S.S. Yang, Y. Qin, B. Chen, V.O. Özçelik, C.E. White, Y. Shen, S.S. Yang, S. Tongay, Novel surface molecular functionalization route to enhance environmental stability of tellurium-containing 2D layers, ACS Appl. Mater. Interfaces 9 (2017) 44625–44631, https://doi.org/10.1021/acsami.7b14873.
[21] R. Ma, H. Zhang, Y. Yoo, Z.P. Degregorio, L. Jin, P. Golani, J. Ghasemi Azadani, T. Low, J.E. Johns, L.A. Bendersky, A.V. Davydov, S.J. Koester, MoTe2 lateral homojunction field-effect transistors fabricated using flux-controlled phase engineering, ACS Nano 13 (2019) 8035–8046, https://doi.org/10.1021/acsnano.9b02785.
[22] J.P. Fraser, L. Masaityte, J. Zhang, S. Laing, J.C. Moreno-López, A.F. McKenzie, J.C. McGlynn, V. Panchal, D. Graham, O. Kazakova, T. Pichler, D.A. MacLaren, D.A.J. Moran, A.Y. Ganin, Selective phase growth and precise-layer control in MoTe2, Commun. Mater. 1 (2020) 1–9, https://doi.org/10.1038/s43246-020-00048-4.
[23] S. Pace, L. Martini, D. Convertino, D.H. Keum, S. Forti, S. Pezzini, F. Fabbri, V. Mišeikis, C. Coletti, Synthesis of large-scale monolayer 1t′-MoTe2and its stabilization via scalable hBN encapsulation, ACS Nano 15 (2021) 4213–4225, https://doi.org/10.1021/acsnano.0c05936.
[24] R. Steeno, M.C. Rodríguez González, S. Eyley, W. Thielemans, K.S. Mali, S. De Feyter, Covalent functionalization of carbon surfaces: diaryliodonium versus aryldiazonium chemistry, Chem. Mater. 32 (2020) 5246–5255, https://doi.org/10.1021/acs.chemmater.0c01393.
[25] L. Koefoed, S. US Pedersen, K. Daasbjerg, Grafting of aryl diazonium, iodonium, and sulfonium salts in unusual patterns by exploiting the potential gradient in bipolar electrochemistry, Chemelectrochem 3 (2016) 495–501, https://doi.org/10.1002/celc.201500512.
[26] E. Miliutina, O. Guselnikova, N.S. Soldatova, P. Bainova, R. Elashnikov, P. Fitl, T. Kurten, M.S. Yusubov, V. Švorčík, R.R. Valiev, M.M. Chehimi, O. Lyutakov, P.S. Postnikov, Can plasmon change reaction path? Decomposition of unsymmetrical iodonium salts as an organic probe, J. Phys. Chem. Lett. 11 (2020) 5770–5776, https://doi.org/10.1021/acs.jpclett.0c01350.
[27] O. Guselnikova, E. Miliutina, R. Elashnikov, V. Burtsev, M.M. Chehimi, V. Svorcik, M. Yusubov, O. Lyutakov, P. Postnikov, Chemical modification of gold surface via UV-generated aryl radicals derived 3,5-bis(trifluoromethyl) phenyl)iodonium salt, Prog. Org. Coating 136 (2019) 105211, https://doi.org/10.1016/j.porgcoat.2019.105211.
[28] E. Miliutina, O. Guselnikova, P. Bainova, Y. Kalachyova, R. Elashnikov, M.S. Yusubov, V.V. Zhdankin, P. Postnikov, V. Švorčík, O. Lyutakov, Plasmon-Assisted activation and grafting by iodonium salt: functionalization of optical fiber surface, Adv. Mater. Interface 5 (2018) 1800725, https://doi.org/10.1002/admi.201800725.
[29] R.A. Schäfer, K. Weber, M. Koleśnik-Gray, F. Hauke, V. Krstić, B. Meyer, A. Hirsch, Substrate-modulated reductive graphene functionalization, Angew. Chem. Int. Ed. 55 (2016) 14858–14862, https://doi.org/10.1002/anie.201607427.
[30] K.R. Nandanapalli, D. Mudusu, S. Lee, Functionalization of graphene layers and advancements in device applications, Carbon N. Y. 152 (2019) 954–985, https://doi.org/10.1016/j.carbon.2019.06.081.
[31] L. Yang, H. Wu, W. Zhang, Z. Chen, J. Li, X. Lou, Z. Xie, R. Zhu, H. Chang, Anomalous oxidation and its effect on electrical transport originating from surface chemical instability in large-area, few-layer 1T′-MoTe2 films, Nanoscale 10 (2018) 19906–19915, https://doi.org/10.1039/C8NR05699D.
[32] A.A.L. Ahmad, J.B. Marutheri Parambath, P.S. Postnikov, O. Guselnikova, M.M. Chehimi, M.R.M. Bruce, A.E. Bruce, A.A. Mohamed, Conceptual developments of aryldiazonium salts as modifiers for gold colloids and surfaces, Langmuir 37 (2021) 8897–8907, https://doi.org/10.1021/acs.langmuir.1c00884.
[33] N. Peimyoo, W. Yang, J. Shang, X. Shen, Y. Wang, T. Yu, Chemically driven tunable light emission of charged and neutral excitons in monolayer WS2, ACS Nano 8 (2014) 11320–11329, https://doi.org/10.1021/nn504196n.
[34] S. Wild, X.T. Dinh, H. Maid, F. Hauke, G. Abellán, A. Hirsch, Quantifying the covalent functionalization of black phosphorus, Angew. Chem. Int. Ed. 59 (2020) 20230–20234, https://doi.org/10.1002/anie.202008646.
[35] M.W. Iqbal, K. Shahzad, R. Akbar, G. Hussain, A review on Raman finger prints of doping and strain effect in TMDCs, Microelectron. Eng. 219 (2020) 111152, https://doi.org/10.1016/j.mee.2019.111152.
[36] H. Gehan, L. Fillaud, M.M. Chehimi, J. Aubard, A. Hohenau, N. Felidj, C. Mangeney, Thermo-induced electromagnetic coupling in gold/polymer hybrid plasmonic structures probed by surface-enhanced Raman scattering, ACS Nano 4 (2010) 6491–6500, https://doi.org/10.1021/nn101451q.
[37] R.I. Gearba, K.M. Mueller, P.A. Veneman, B.J. Holliday, C.K. Chan, K.J. Stevenson, Atom-scale covalent electrochemical modification of single-layer graphene on

SiC substrates by diaryliodonium salts, J. Electroanal. Chem. 753 (2015) 9–15, https://doi.org/10.1016/j.jelechem.2015.05.009.
[38] A. Mattiuzzi, Q. Lenne, J. Carvalho Padilha, L. Troian-Gautier, Y.R. Leroux, I. Jabin, C. Lagrost, Strategies for the formation of monolayers from diazonium salts: unconventional Grafting media, unconventional building blocks, Front. Chem. 8 (2020) 559, https://doi.org/10.3389/fchem.2020.00559.
[39] J. Médard, C. Combellas, F. Kanoufi, J. Pinson, J. Chauvin, A. Deronzier, Patterning surfaces through photografting of iodonium salts, J. Phys. Chem. C 122 (2018) 19722–19730, https://doi.org/10.1021/acs.jpcc.8b06541.
[40] A. Olshtrem, O. Guselnikova, P. Postnikov, A. Trelin, M. Yusubov, Y. Kalachyova, L. Lapcak, M. Cieslar, P. Ulbrich, V. Svorcik, O. Lyutakov, Plasmon-assisted grafting of anisotropic nanoparticles - spatially selective surface modification and the creation of amphiphilic SERS nanoprobes, Nanoscale 12 (2020) 14581–14588, https://doi.org/10.1039/d0nr02934c.
[41] H. Zhu, Y. Yang, K. Wu, T. Lian, Charge transfer dynamics from photoexcited semiconductor quantum dots, Annu. Rev. Phys. Chem. 67 (2016) 259–281, https://doi.org/10.1146/annurev-physchem-040215-112128.
[42] J. Kabatc, K. Iwińska, A. Balcerak, D. Kwiatkowska, A. Skotnicka, Z. Czech, M. Bartkowiak, Onium salts improve the kinetics of photopolymerization of acrylate activated with visible light, RSC Adv. 10 (2020) 24817–24829, https://doi.org/10.1039/D0RA03818K.
[43] C. Combellas, F. Kanoufi, J. Pinson, F.I. Podvorica, Sterically hindered diazonium salts for the grafting of a monolayer on metals, J. Am. Chem. Soc. 130 (2008) 8576–8577, https://doi.org/10.1021/ja8018912.
[44] D.-S. Liu, J. Wu, H. Xu, Z. Wang, Emerging light-emitting materials for photonic integration, Adv. Mater. 33 (2021) 2003733, https://doi.org/10.1002/adma.202003733.
[45] H. Zhu, Q. Wang, L. Cheng, R. Addou, J. Kim, M.J. Kim, R.M. Wallace, Defects and surface structural stability of $MoTe_2$ under vacuum annealing, ACS Nano 11 (2017) 11005–11014, https://doi.org/10.1021/acsnano.7b04984.
[46] Q. Li, Q. Zhou, L. Shi, Q. Chen, J. Wang, Recent advances in oxidation and degradation mechanisms of ultrathin 2D materials under ambient conditions and their passivation strategies, J. Mater. Chem. A 7 (2019) 4291–4312, https://doi.org/10.1039/c8ta10306b.
[47] H. Fang, J. Liu, Q. Lin, R. Su, Y. Wei, T.F. Krauss, J. Li, Y. Wang, X. Wang, Laser-like emission from a sandwiched $MoTe_2$ heterostructure on a silicon single-mode resonator, Adv. Opt. Mater. (2019) 1900538, https://doi.org/10.1002/adom.201900538.
[48] H. Zhu, R. Addou, Q. Wang, Y. Nie, K. Cho, M.J. Kim, R.M. Wallace, Surface and interfacial study of atomic layer deposited Al2O3 on MoTe2 and WTe2, Nanotechnology 31 (2019) 55704, https://doi.org/10.1088/1361-6528/ab4e44.
[49] C.D. Christiansen, L.A. Sørensen, T. Lund, Modification of fluorine-doped tin oxide-electrodes by electrochemical reduction of di(4-nitrophenyl)iodonium tetrafluoroborate - and its application as a photo-anode in dye-sensitized solar cells, J. Electroanal. Chem. 809 (2018) 44–51, https://doi.org/10.1016/j.jelechem.2017.12.050.
[50] S. Tang, C. Zhang, C. Jia, H. Ryu, C. Hwang, M. Hashimoto, D. Lu, Z. Liu, T.P. Devereaux, Z.-X. Shen, S.-K. Mo, Electronic structure of monolayer 1T′-MoTe2 grown by molecular beam epitaxy, Apl. Mater. 6 (2017) 26601, https://doi.org/10.1063/1.5004700.
[51] M.S. Strano, C.A. Dyke, M.L. Usrey, P.W. Barone, M.J. Allen, H. Shan, C. Kittrell, R.H. Hauge, J.M. Tour, R.E. Smalley, Electronic structure control of single-waited carbon nanotube functionalization, Science (80) 301 (2003) 1519–1522, https://doi.org/10.1126/science.1087691.
[52] R.D. Rodriguez, A. Khalelov, P.S. Postnikov, A. Lipovka, E. Dorozhko, I. Amin, G.V. Murastov, J.J. Chen, W. Sheng, M.E. Trusova, M.M. Chehimi, E. Sheremet, Beyond graphene oxide: laser engineering functionalized graphene for flexible electronics, Mater. Horizons. 7 (2020) 1030–1041, https://doi.org/10.1039/c9mh01950b.